International Journal for Modern Trends in Science and Technology, 8(07): 27-34, 2022

ISSN: 2455-3778 online
DOI: https://doi.org/10.46501/IJMTST0807005
Available online at: http://www.ijmtst.com/vol8issue07.html

Wire Arc Additive Manufacturing of AA 7075 Correlation of Arc Mode Microstructure & Mechanical Properties

P. Rohith Krishna, P. Murali Krishna Yadav, M. Naga Uday Kiran, Vivek Kumar and V. V. Ravi Kumar

Department of Mechanical Engineering, N S Raju Institute of Technology (NSRIT), Visakhapatnam, A.P, India.

To Cite this Article
P. Rohith Krishna, P. Murali Krishna Yadav, M. Naga Uday Kiran, Vivek Kumar and V. V. Ravi Kumar. Wire Arc Additive Manufacturing of AA 7075 Correlation of Arc Mode Microstructure & Mechanical Properties. International Journal for Modern Trends in Science and Technology 2022, 8(07), pp. 27-34. https://doi.org/10.46501/IJMTST0807005

Article Info
Received: 27 May 2022; Accepted: 25 June 2022; Published: 28 June 2022.

ABSTRACT

Wire arc additive manufacturing (WAAM) is a promising approach to producing large-scale metal structures. The investigation on the WAAM of aluminum alloys and Titanium alloys has lasted for over 17 years and covered multiple alloy systems. However, fundamental research on the WAAM of quaternary Al-Zn-Mg-Cu alloys is still lacking. This review paper focuses on understanding the micro structural characteristics and mechanical properties of an ultra-high-strength alloy fabricated by WAAM. Results indicate that a single deposition layer consists of two types of columnar grains with different micrographs and origins. Nanoscale second phases are observed to precipitate during the manufacturing process with location-dependent sizes and volume fractions due to different thermal histories. The micro hardness of the cross-section exhibits a special un-uniform distribution between 75-164 HV0.2 from the substrate to the top of the component. The WAAM deposited component shows higher overall tensile properties than the as-fabricated spray formed counterpart. The average yield strength and ultimate strength are higher in the vertical direction than in the horizontal direction, while the difference in elongation is small. Wire arc additive manufacturing (WAAM) offers a promising alternative to traditional subtractive manufacturing of metallic components, particularly in the case of large Ti6Al4V structures for the aerospace sector that feature high buy-to-fly ratios. This study investigates the influence of heat accumulation on bead formation, arc stability, and metal transfer behaviour during the manufacture of Ti6Al4V with the gas tungsten wire arc additive manufacturing (GT-WAAM) using localized gas shielding. An infrared pyrometer is used to measure the in-situ inter pass temperature which is a key factor in determining the heat accumulation. Arc stability and metal transfer behaviour are monitored by means of a high speed camera. The results show that due to the various thermal dissipation paths along the building height, there exists a significant difference in temperature variation between substrate and in-situ layer.

KEYWORDS: Additive Manufacturing; AA 7075; Microstructure; Mechanical Property, Heat accumulation; Arc shape; Metal transfer.

1. INTRODUCTION

Additive manufacturing transforms the fabrication of a structurally complicated three-dimensional (3D) component into stepwise additions of thin material layers guided by a digital model [1, 2]. Additive manufacturing enables the fabrication of structurally

complex components without using a mold, which significantly improves production efficiency and manufacturing flexibility [3, 4]. Laser beams, electron beams, and electric arcs are commonly used heat sources during additive manufacturing of metallic components [5-7]. When laser beams or electron beams are selected as the heat source, the energy control is accurate, and the component shape is relatively precise [8, 9]. Therefore, investigations regarding additive manufacturing based on laser and electron beams are thorough [10-12]. Direct energy deposition and power bed fusion are the general additive manufacturing processes used when laser beams or electron beams are selected as the heat source [13, 14].

Wire arc additive manufacturing (WAAM) adopts an arc as the heat source and metal wire as the feedstock material. Generally, the primary cost of the metal wire is approximately 10% of the same weight of metal powder. During the WAAM process, the metal wire is heated, melted, and then transferred to the melt pool and then solidifies at the melt pool boundary and forms digitally designed components [15, 16]. WAAM is a kind of droplet based additive manufacturing process, which is very promising for the direct fabrication of complex thin walled parts [17, 18]. WAAM features a high deposition rate, which is suitable for fabricating large scale components [19,20]. Furthermore, WAAM features advantages such as low cost and low wastage rate, and thus WAAM is an advantageous alternative additive manufacturing process to other methods based on laser and electron beams [21,22]. The dominant factor that affects the component morphology, microstructure, and mechanical properties during WAAM is the heat input. However, differences in heat input exist when different arc modes are adopted even if the wire feeding rate is held constant.

Another particular phenomenon found in WAAM is the transfer of liquid droplets across the arc from the wire electrode to the melt pool [23, 24]. The liquid droplet temperature is higher than the solidus temperature, and part of heat is transferred to the melt pool by the liquid droplet [25]. However, differences in liquid droplet transfer exist when different metal transfer modes are adopted even if the wire feeding rate is held constant. Therefore, what is essential but seldom reported in the literature is to reveal what and how the metal transfer mode affects the component morphology, microstructure, and mechanical properties during WAAM. Cong et al. [26] systematically investigated the effects of different metal transfer modes during the cold metal transfer (CMT) process on the porosity characteristics of additively manufactured Al-6.3%Cu alloys, and their results indicated that heat input is one of the critical factors that enables the CMT pulse advanced (CMT-PADV) process to control the porosity rate. Luo et al. [27] conducted WAAM on aluminum alloys using pulsed arcs and non pulsed arcs, and their results indicated that pulsed arcs can achieve higher droplet transfer frequencies and that the size of the droplet in the pulsed arc approach is smaller than that in the non pulsed arc approach. Although some characteristics of WAAM under various arc modes have been documented in the literature, the component morphology, integrity, microstructure, and mechanical properties are not comprehensively demonstrated or understood. Stainless steel 316L is a kind of austenitic stainless steel that is widely used in marine and offshore equipment, automobiles, and nuclear reactors due to its outstanding corrosion resistance, high strength, high ductility, and relatively low cost [28,29]. Arc current and arc voltage data were collected during the additive manufacturing process to evaluate the manufacturing process stability. X-ray CT tests were conducted on tensile samples of the component to evaluate the structural integrity of the manufactured component. The microstructures at different locations in the components were characterized to reveal the relationship between the arc modes and microstructures. Tensile tests were conducted on the different locations of the components, and the fracture morphologies were analyzed to reveal the relationships between the metal transfer modes and mechanical properties.

A major benefit of the WAAM process relates to the low capital investment, as the components of a WAAM machine may be derived of open source equipment, sourced from an array of suppliers in the mature welding industry [30]. The processing characteristics may also make the WAAM process preferable compared to the alternative fusion sources. For example, WAAM does not does not need a vacuum environment to operate as required in electron beam based methods [31]. As such, prolonged set up and ramp down times which can lead to over-aging in precipitate hardened

materials can be avoided [32]. Whilst inert shielding gas may not be required in electron beam DED to avoid atmospheric contamination, there is an elevated susceptibility to element depletion and evaporation during processing [33]. In comparison to laser based methods, the use of the electrical arc offers a higher efficiency fusion source [34]. This is of benefit from an energy consumption perspective, in particular, for reflective metal alloys of poor laser coupling efficiency such as aluminium, copper [35] and magnesium [36]. With typical layer heights of 1–2 mm, surface waviness of 500 μm [37] and deposition rates up to 10 kg/hr, WAAM productivity and material removed is similar to laser based and electron beam-based DED approaches. Research and developments have allowed the WAAM process to become highly capable in a number of materials, including aerospace titanium alloy Ti-6Al-4 V and nickel bronze, where static mechanical properties close to those found in wrought and cast can be produced [38]. Present there are several commercial WAAM machine manufacturers and/or service providers able to produce WAAM components in a number of materials. However, high quality production of WAAM parts is only achievable when the specific materials processing challenges related to the high-levels of heat input of the WAAM process are addressed. Williams, et al. [39] and Ding et al. regarded the management of the high levels of residual stress and distortion as the primary heat related material processing challenge in WAAM. Ding et al. considered the surface finish of WAAM parts another major concern to dimensional compliance as well as premature part failure. Practical methods of mitigating these issues were presented, but were limited in scope primarily to build strategies for the management of residual stress. Pan et al. [40] Summarized of static mechanical properties achieved in WAAM research, reporting the welding technology and processing condition, e.g. heat treated, interlayer cooling etc. however, the mechanisms of material property improvements were not discussed. This project identifies the full range of materials processing challenges in WAAM. The primary process selections and ancillary processes that may be used in WAAM are classified by the authors and the strategies in which they may be deployed to overcome these challenges are presented. Finally, future challenges and opportunities in the area of WAAM are identified. Owing to the influences of heat accumulation, the interlayer surface oxidation and bead geometries vary along the building direction, especially for the first few layers of the deposited wall, which lead to variation in arc shape and metal transfer behaviour. The research outcome provides a better understanding of the effects of heat accumulation on deposition stability during WAAM process, which benefits future process optimization and control.

2. EXPERIMENTAL WORK

2.1 Material and methods

The 7055-Aluminum alloy flat plates join was with the WAAM system shown in Figure 1, which consisted of a Miller Dynasty 350 GTAW power supply, a GTAW torch, a preheating platform, a three-degrees-of-freedom moving table, a wire feeder, and a control system. For the WAAM process, the preheating platform was heated to a certain interlayer temperature (80 ℃ in this experiment). When depositing a single layer, the welding torch remained static, while the moving table traversed a pre-set trajectory. When one layer was deposited, the welding torch was lifted to the next layer, and the moving table returned to the starting place. The temperature of the layer was detected with a Tachyon 1024 μcore thermal imager. When it decreased to the pre-set level, the next layer was deposited. The deposition parameters used in this work are presented in Table 1. SAL7055 aluminum wires with a diameter of 1.2 mm were used as feedstock.

Figure 1 WAAM system

Table 1 Deposition parameters

EP Current (A)	EN Current (A)	EN-EP Balance (%)	AC Frequency (Hz)	Arc length (mm)	Deposition speed (cm/min)	Wire feed speed (cm/min)	Inter-pass temperature (°C)
220	120	80	105	4	10	130	80

A single-pass multilayer component was manufactured with the WAAM system, as shown in Figure 2. The length, width, and height are 250 mm, 10 mm and 55 mm, respectively. Cross-section of the fabricated component.

Figure 2 Single-pass multilayer component: (a) The fabricated component,

For the tests on the tensile properties, samples were cut in two directions: horizontal and vertical, as shown in Figure 3. Eight test samples were cut for each direction. All samples were polished with metallographic abrasive paper. Tensile tests were carried out with Instron-5569 at room temperature with a loading velocity of 2 mm/min. Sample fractures were observed with an FEI Quanta 200FEG SEM to investigate the fracture mechanism.

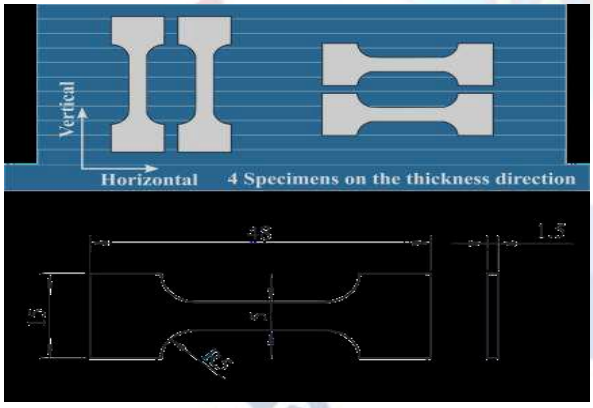

Figure 3. Cutting locations and dimensions of tensile

3. RESULT AND DISCUSSION

3.1 Second phase and distribution of alloy elements

To characterize the distribution of alloy elements in as-deposited 7055-Al at the micro-scale, electron probe micro analysis (EPMA) was performed in the middle part of the cross-section. As shown in Figure 4, the results indicate severe element segregations. The solute distribution coefficients of main alloy elements Zn, Mg, and Cu are less than 1.0. Thus, during non-equilibrium crystallization, they enrich on grain boundaries and dendritic boundaries to form residual second phases. This kind of distribution is detrimental to the mechanical properties and corrosion resistance because intermetallic at this scale is brittle and has a large electric potential difference with the matrix Several studies on cast AA-7055 aluminum alloy have proven that the main second phases in the solidified state are T (Al2Mg3Zn3), η(Mg(Zn,Cu,Al)2), S(Al2CuMg), and θ(Al2Cu). We conducted microregion X-ray diffraction (XRD) in the middle part of the cross-section. As shown in Figure 5, the diffraction peaks of α-Al and η (Mg (Zn,Cu,Al)2) are identified.

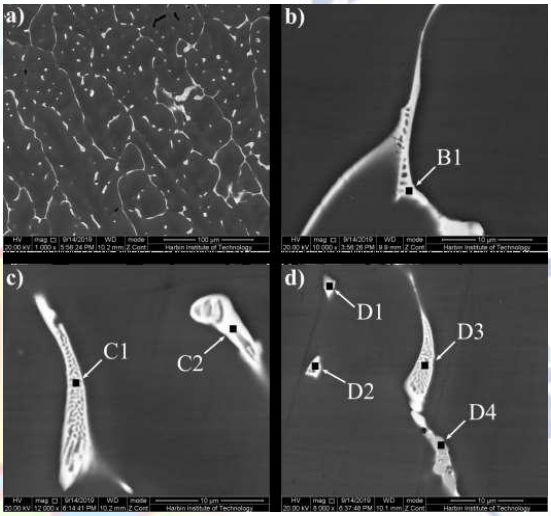

Fig.4. SEM images of as-deposited 7055-Al: (a) Low-magnification BSE image of the middle part on the cross-section, (b) second phases on grain boundaries, (c) second phases inside grains, (d) grey phases wrapped by white phases.

SEM and EDS were used to characterize these second phases. Figure 4.a shows a low magnification backscattered electron (BSE) image of the middle part of the cross-section. These second phases are continuously distributed on grain boundaries, forming a complex network. Skeletal structures are observed within the different phases, as shown in Figures 4.b-d. This indicates that they are eutectics with the matrix. As shown in Figure 4.d, a small number of gray phases are wrapped by white phases. EDS analysis was conducted on seven points within the second phase, marked in Figure 4. The chemical constituents of those white phases are similar. The proportions of Zn, Mg are almost identical, while the proportion of Cu is lower, and the content of Al is high. It is difficult to determine

the definite phase types from the tested chemical compositions without evidence of crystal structures as the alloy elements dissolve during non-equilibrium solidification. The gray phases have a high content of the impurity element Fe, and the Cu content is higher than the Zn and Mg contents. Thus, they can be inferred to be Al7Cu2Fe.

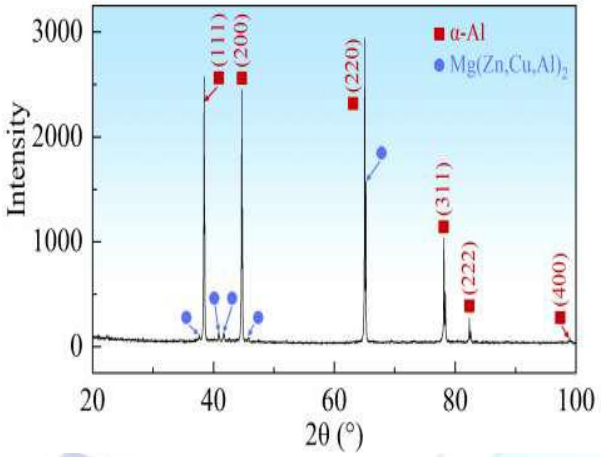

Figure 5 Microregion XRD of as-deposited 7055-Al

3.2 Mechanical Properties

3.2.1 Microhardness

Microhardness tests were carried out on the cross-section of as-deposited 7055- Al to evaluate the micromechanical properties. We focused on the hardness uniformity at different layers. An interval of 1 mm was chosen along the vertical direction, and 5 points were tested at each location. The hardness distribution is shown in Figure 7. The hardness increases significantly from the bottom to the top of the cross-section. The chemical composition of the substrate is different, due to the dilution effect, the first few points have the lowest hardness. Below a height of 20 mm, the hardness distribution stabilizes at around 75 HV0.2. However, it increases at a rate of 3.8 HV0.2/mm to 164 HV0.2 up to a height of 45 mm. Above 45mm, the hardness decreases gradually to 136 HV0.2. This non-uniform hardness distribution significantly differs from that of other aluminum alloys fabricated by WAAM.

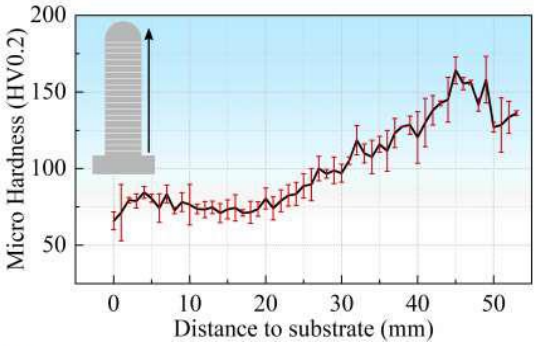

Figure 6 Hardness distribution on the cross-section

The hardness distribution can be explained by the evolution of the second phase. For the top region above 45 mm, the alloy elements are dissolved in the Al matrix, and the strengthening mechanism is mainly solution strengthening. As discussed in the second phase can precipitate out during the deposition process for as-deposited 7055-Al. For the lower part of the component, the strengthening mechanism gradually changes to precipitation strengthening. Thus, we observed the hardness increasing from the top of the specimen to the height of 45 mm after several subsequent thermal cycles. The strengthening effect of second phases with incoherent sizes can be expressed by the Orowan mechanism : where τc is the shearing stress required by dislocations, f and R are the volume fraction and radius of the precipitates, G is the shear modulus, ν is the Poisson's ratio, b is the Burgers vector, and $r0$ is the radius of the dislocation core. The model indicates that the strengthening effects are highly sensitive to the sizes and volume fractions of the second phase. However, because the subsequent thermal cycles during WAAM can be regarded as isothermal aging with relatively high peak temperatures for the deposited metal, the growth rate of the second phase after nucleation is very fast . This increases the growth in size and reduces the volume fractions, which further degrades the strengthening effects. Thus, the hardness decreases significantly from the height of 45 mm to 20 mm and finally reaching a stable state

3.2.2 Tensile tests

Tensile tests were carried out on as-deposited 7055-Al to evaluate the macro mechanical properties. Samples were tested in both horizontal and vertical directions to compare the anisotropies that have been observed in other as-deposited materials. Figure 8

shows the tensile properties. We labeled the tensile test samples by the test direction and sample ID. For example, H-3 represents the third test sample in the horizontal direction. Figure 8a and b show the tensile curves of the 16 specimens, while Figure 8 c and d give the strength and elongations obtained from tensile curves. The average yield stress, tensile stress, and elongation of as-deposited 7055-Al are 148.3±15.9 MPa, 230.7±12.0 MPa, and 3.3±1.0 %, respectively. The results from different samples show significant dispersion, especially for elongation. This indicates that the as-deposited 7055-Al is not sufficiently homogeneous. The average yield strength and ultimate strength are 16.8 % and 7.6 % higher in the vertical direction than in the horizontal direction. In contrast, the difference in average elongation according to direction is small, considering the large fluctuations in the test data.

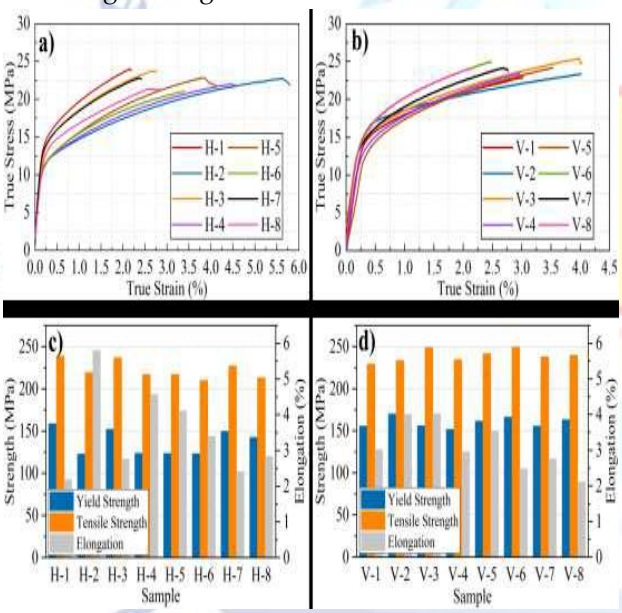

Figure 7 Tensile properties of as-deposited 7055-Al: tensile curves of (a) horizontal and (b) vertical specimens, strengths and elongations of (c) horizontal and (d) vertical specimens

Table 2 shows a comparison of tensile properties between the as-deposited specimen and 7055-Al in other states. Compared with other as-fabricated states, the WAAM deposited 7055-Al exhibits greater strength and elongation than the spray formed counterpart without further extrusions, and higher elongation than the direct chilling cast counterpart . However, compared with those that have been subjected to hot working and heat treatments, the WAAM deposited 7055-Al shows inferior overall tensile properties. There are two reasons for the poor performance. On the one hand, there are ubiquitous porosities in the as-deposited has been observed during WAAM, the solutes are depleted by the large second phases. The solution strengthening and precipitating strengthening effects are still weaker than the heat-treated specimens.

Table 2 Mechanical properties of 7055-Al in different states

Manufacturing Technique	Heat treatment	Temperature	Yield Strength (MPa)	Tensile Strength (MPa)	Elongation (%)
Waam	CAST		148	230	3.2
Waam	Solution: 450°C/24 h Aging: 120°C /12h	T6	608	667	10
Waam	Solution:470°C /24h Aging: 120°C /12h	T6	562	620	11
Waam	Solution: 475°C /1h Aging: 120°C /24h Regression: 160°C /0.5h Re-aging: 120°C /24h	T77	720	732	7.2

The profiles of the tensile test specimens are observed to examine the crack propagation path. As illustrated in Figure 8 a and b, broken second phases and porosities are observed distributed along the crack propagation path for samples in both horizontal and vertical directions. Figure 8c shows a second crack initiates from continuous second phases and propagates along the grain boundary. Moreover, porosities are found connected by the second crack in Figure 8d. The second crack propagates along the continuous second phases between porosities. The above observation reveals that the continuous second phases and porosities are weaknesses of the WAAM deposited

7055-Al. They can act as crack sources individually. In addition, porosities are geometric discontinuities themselves, which may further accelerate the crack propagation by connecting the cracks initiate from second phases.

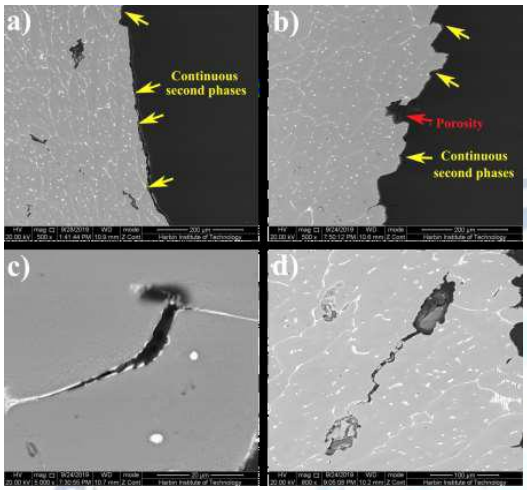

Figure 8 SEM images of side fracture surfaces: low magnification BSE image for the side fracture of (a) horizontal and (b) vertical specimens; (c) secondary crack initiates from net-shaped second phases; (d) porosities play a vital role in crack propagation by connecting cracks from second phases.

4. CONCLUSIONS

In this review paper the Al-Zn-Mg-Cu aluminum alloy 7055-Al was successfully fabricated by GTAW-based WAAM. The microstructure characteristics and mechanical properties were comprehensively analyzed for the first time.

The conclusions are summarized as follows:

(1) A single deposition layer consists of two types of columnar grains originating from the bottom fusion lines and the starting position of the deposition layer. During the subsequent deposition, columnar grains originating from the starting position of the deposition layer are partially remelted, and columnar grains originating from the bottom fusion lines mostly survive. This results in the periodicity of the grain morphologies observed in different sections.

(2) Mg(Zn, Cu, Al)2 and Al7Cu2Fe Precipitation of nanoscale second phases is found to occur during the manufacturing process. Under the heat influences of the subsequent deposition process, nanoscale second phases nucleate in the supersaturated matrix and grow larger than 1.0 μm. These second phases are identified by HRTEM, HAADF, and nanoscale EDS as T(Al2Mg3Zn3) and η(Mg(Zn, Cu, Al)2) phases.

(3) The microhardness exhibits a special non-uniform distribution on the cross- section because of different sizes and volume fractions of second phases along the vertical direction. The hardness stabilizes near 75 HV0.2 below a height of 20 mm and then increases with height at a rate of 3.8 HV0.2/mm to 164 HV0.2. Above 45mm, the hardness decreases to 136 HV0.2.

(4) The average yield stress, tensile stress, and elongation of as-deposited 7055- Al are 148.3±15.9 MPa, 230.7±12.0 MPa, and 3.3±1.0%, respectively. The average yield strength and ultimate strength are 16.8% and 7.6% higher in the vertical direction than in the horizontal direction, while the difference in elongation is small. The WAAM deposited component shows higher overall tensile properties than the as fabricated spray formed counterpart. Fracture path of the as-deposited 7055-Al is predominantly intergranular with some transgranular contributions, while the fracture mode is the cleavage fracture. Continuous second phases and porosities are the major weaknesses.

Conflict of interest statement

Authors declare that they do not have any conflict of interest.

REFERENCES

[1] J.R. Tumbleston, D. Shirvanyants, N. Ermoshkin, R. Janusziewicz, A.R. Johnson, D. Kelly, K. Chen, R. Pinschmidt, J.P. Rolland, A. Ermoshkin, E.T. Samulski, J.M. DeSimone, Continuous liquid interface production of 3D objects, Science 347 (2018) 1349–1352.

[2] D.L. Bourell, Perspectives on additive manufacturing, Ann. Rev. Mater. Res. 46 (2016) 1–1

[3] R.L. Truby, J.A. Lewis, Printing soft matter in three dimensions, Nature 540 (2016) 371–37

[4] J.H. Martin, B.D. Yahata, J.M. Hundley, J.A. Mayer, T.A. Schaedler, T.M. Pollock, 3D printing of high-strength aluminium alloys, Nature 549 (2017) 365–369.

[5] Z. Gan, G. Yu, X. He, S. Li, Numerical simulation of thermal behavior and multi component mass transfer in direct laser deposition of Co-base alloy on steel, Int. J. Heat. Mass Transf. 104 (2017) 28–38.

[6] Y.S. Lee, M.M. Kirka, R.B. Dinwiddie, N. Raghavan, J. Turner, R.R. Dehoff, S.S. Babu, Role of scan strategies on thermal gradient

and solidification rate in electron beam powder bed fusion, Addit. Manuf. 22 (2018) 516–527.
[7] W. Ou, T. Mukherjee, G.L. Knapp, Y. Wei, T. DebRoy, Fusion zone geometries, cooling rates and solidification parameters during wire arc additive manufacturing, Int. J. Heat. Mass Transf. 127 (2018) 1084–1094.
[8] M. Ziętala, T. Durejko, M. Polański, I. Kunce, T. Płociński, W. Zieliński, M. Łazińska, W. Stępniowski, T. Czujko, K.J. Kurzydłowski, Z. Bojar, The microstructure, mechanical properties and corrosion resistance of 316L stainless steel fabricated using laser engineered net shaping, Mater. Sci. Eng. A 677 (2016) 1–10.
[9] D.D. Gu, W. Meiners, K. Wissenbach, R. Poprawe, Laser additive manufacturing of metallic components: materials, processes and mechanisms, Int. Mater. Rev. 57 (2012) 133–164.
[10] T. DebRoy, H.L. Wei, J.S. Zuback, T. Mukherjee, J.W. Elmer, J.O. Milewski, A.M. Beese, A. Wilson-Heid, A. De, W. Zhang, Additive manufacturing of metallic components – process, structure and properties, Prog. Mater. Sci. 92 (2018) 112–224.
[11] C. Körner, Additive manufacturing of metallic components by selective electron beam melting — a review, Int. Mater. Rev. 61 (2016) 361–377.
[12] D. Herzog, V. Seyda, E. Wycisk, C. Emmelmann, Additive manufacturing of metals, Acta Mater. 117 (2016) 371–392.
[13] G.L. Knapp, T. Mukherjee, J.S. Zuback, H.L. Wei, T.A. Palmer, A. De, T. DebRoy, Building blocks for a digital twin of additive manufacturing, Acta Mater. 135 (2017) 390–399.
[14] H.J. Willy, X. Li, Z. Chen, T.S. Herng, S. Chang, C.Y.A. Ong, C. Li, J. Ding, Model of laser energy absorption adjusted to optical measurements with effective use in finite element simulation of selective laser melting, Mater. Des. 157 (2018) 24–34.
[15] W.E. Frazier, Metal additive manufacturing: a review, J. Mater. Eng. Perform. 23 (2014) 1917–1928.
[16] A. Horgar, H. Fostervoll, B. Nyhus, X. Ren, M. Eriksson, O.M. Akselsen, Additive manufacturing using WAAM with AA5183 wire, J. Mater. Process. Technol. 259 (2018) 68–74.
[17] H. Yi, L. Qi, J. Luo, N. Li, Hole-defects in soluble core assisted aluminum droplet printing: metallurgical mechanisms and elimination methods, Appl. Therm. Eng. 148 (2019) 1183–1193.
[18] H. Yi, L. Qi, J. Luo, D. Zhang, H. Li, X. Hou, Effect of the surface morphology of solidified droplet on remelting between neighboring aluminum droplets, Int. J. Mach. Tools Manuf. 130–131 (2018) 1–11.
[19] J. Ding, P. Colegrove, F. Martina, S. Williams, R. Wiktorowicz, M.R. Palt, Development of a laminar flow local shielding device for wire+arc additive manufacture, J. Mater. Process. Technol. 226 (2015) 99–105.
[20] J. Xiong, Y. Lei, H. Chen, G. Zhang, Fabrication of inclined thin-walled parts in multi-layer single-pass GMAW-based additive manufacturing with flat position deposition, J. Mater. Process. Technol. 240 (2017) 397–403.
[21] J. Zhang, X. Zhang, X. Wang, J. Ding, Y. Traoré, S. Paddea, S. Williams, Crack path selection at the interface of wrought and wire+arc additive manufactured Ti–6Al–4V, Mater. Des. 104 (2016) 365–375.
[22] D. Yang, C. He, G. Zhang, Forming characteristics of thin-wall steel parts by double electrode GMAW based additive manufacturing, J. Mater. Process. Technol. 227 (2016) 153–160.
[23] A. Scotti, V. Ponomarev, W. Lucas, Interchangeable metal transfer phenomenon in GMA welding: features, mechanisms, classification, J. Mater. Process. Technol. 214 (2014) 2488–2496.
[24] A. Scotti, V. Ponomarev, W. Lucas, A scientific application oriented classification for metal transfer modes in GMA welding, J. Mater. Process. Technol. 212 (2012) 1406–1413.
[25] H. Yi, L. Qi, J. Luo, D. Zhang, N. Li, Direct fabrication of metal tubes with high quality inner surfaces via droplet deposition over soluble cores, J. Mater. Process. Technol. 264 (2019) 145–154.
[26] B. Cong, J. Ding, S. Williams, Effect of arc mode in cold metal transfer process on porosity of additively manufactured Al-6.3%Cu alloy, Int. J. Adv. Manuf. Technol. 76 (2015) 1593–1606.
[27] Y. Luo, J. Li, J. Xu, L. Zhu, J. Han, C. Zhang, Influence of pulsed arc on the metal droplet deposited by projected transfer mode in wire-arc additive manufacturing, J. Mater. Process. Technol. 259 (2018) 353–360.
[28] C. Wang, X. Tan, E. Liu, S.B. Tor, Process parameter optimization and mechanical properties for additively manufactured stainless steel 316L parts by selective electron beam melting, Mater. Des. 147 (2018) 157–166.
[29] Y. Zhong, L.-E. Rännar, L. Liu, A. Koptyug, S. Wikman, J. Olsen, D. Cui, Z. Shen, Additive manufacturing of 316L stainless steel by electron beam melting for nuclear fusion applications, J. Nucl. Mater. 486 (2017) 234–245.
[30] G.C. Anzalone, C.L. Zhang, B. Wijnen, P.G. Sanders, J.M. Pearce, A Low-cost Open source metal 3-D printer, IEEE Access. 1 (2013) 803–810.
[31] J.O. Milewski, Lasers, Electron Beams, Plasma Arcs, Additive Manufacturing of Metals, Springer International Publishing, 2017, pp. 85–97.
[32] W.J. Sames, K.A. Unocic, G.W. Helmreich, M.M. Kirka, F. Medina, R.R. Dehoff, S.S. Babu, Feasibility of in situ controlled heat treatment (ISHT) of inconel 718 during electron beam melting additive manufacturing, Addit. Manuf. 13 (2017) 156–165.